

Deep-trapping kinematics of charge carriers in amorphous semiconductors: A theoretical and experimental study

S. O. Kasap, Viswanath Aiyah, B. Polischuk, A. Bhattacharyya, and Z. Liang

Department of Electrical Engineering, University of Saskatchewan, Saskatoon, Canada S7N 0W0

(Received 3 August 1990)

There has been much recent interest in the determination of drift-mobility (μ)–lifetime (τ) products in amorphous semiconductors by various measurement techniques. Although most measurements have utilized time-of-flight types of transient-photoconductivity experiments, xerographic measurements have also been used, since they provide a clear measurement of the residual potential V_R , i.e., the electrostatic potential on the surface of a high-resistivity solid, due to trapped charges in the bulk. This paper identifies and critically examines the theoretical problems involved in the determination of $\mu\tau$ from such xerographic measurements. The deep-trapping model of Kanazawa and Batra, which relates the residual potential to the $\mu\tau$ product, is reformulated by specifically including the effect of the rate of trapping as being proportional to the instantaneous *unoccupied* density of traps. The latter description had been neglected in previous models of deep-trapping kinematics. A partial differential equation is derived that describes the space and time evolution of the electric field within the material. By numerically solving the differential equation and integrating the electric field, the residual potential V_R has been related to the $\mu\tau$ product. It is found that V_R depends not only on the $\mu\tau$ product but also on the capture coefficient to the microscopic mobility ratio, C_i/μ_0 . Universal curves relating V_R to the $\mu\tau$ product and parametric in C_i/μ_0 have been obtained that clearly show the importance of including the effect of trap filling in the theory. Furthermore, it is shown that the $\mu\tau$ product cannot be uniquely determined via xerographic measurements unless $(\epsilon C_i/e\mu_0) \ll 1$, where ϵ is the permittivity of the material. Xerographic first-cycle residual-potential experiments in conjunction with interrupted-field time-of-flight (IFTOF) transient-photoconductivity measurements have been carried out on vacuum-deposited pure *a*-Se and chlorine-doped *a*-Se:0.3 at. % As alloy films to experimentally correlate the residual potential with the $\mu\tau$ values. It is shown that the Kanazawa-Batra universal curve is completely inadequate in describing the present experimental V_R versus $\mu\tau$ data, by as much as a factor of 5, whereas the theory developed herein can account for the experiments, provided that the capture coefficient C_i is $1.22 \times 10^{-7} \text{ cm}^3 \text{ s}^{-1}$. The limitations of the present model and its implications are also addressed. The simple range-limited transport concept of Warter leading to the expression $V_R = L^2/2\mu\tau$ for the residual potential under weak-trapping conditions has been found to predict the residual voltage surprisingly well and to within a factor of 2. By carrying out cycled-up xerographic residual-potential experiments on the same films for which the deep-trapping times have been determined, the capture radius of deep hole traps in *a*-Se and chlorinated *a*-Se:0.3 at. % As films have been determined. Application of ballistic and diffusional trapping models of Street to the IFTOF lifetime and cycled-up residual-potential data imply capture radii of 2–3 Å for both pure *a*-Se and Cl-doped 0.3 at. % As alloys. The first-cycle residual-potential model developed herein in combination with IFTOF results, however, leads to capture radii of ~ 20 and 85 Å for ballistic and diffusional capture, respectively. The results are discussed in terms of valence-alternation-pair (VAP) and intimate-VAP (IVAP) centers in amorphous semiconductors. The energy spectrum of the density of localized midgap states for both *a*-Se and Cl-doped *a*-Se:0.3 at. % As films have been obtained via the xerographic-spectroscopy technique of Abkowitz and Markovics.

I. INTRODUCTION AND BACKGROUND

The performance of many amorphous semiconductor devices, for example, xerographic photoreceptors and solar cells, is directly related to the range of the charge carriers,^{1,2} which is defined as the drift mobility (μ) and lifetime (τ') product, $\mu\tau'$. There has been, therefore, much recent interest in the determination of charge-carrier ranges in amorphous semiconductors by various measurement techniques. Although most measurements have

utilized the time-of-flight type of transient-photoconductivity experiments, xerographic measurements have been also used since they provide a clear measurement of the residual potential, i.e., electrostatic potential on the surface of a high-resistivity solid, due to trapped charges in the bulk.

In xerographic measurements, as illustrated in Fig. 1, the sample is corona charged to a voltage V_0 and then exposed to a short-wavelength (absorption depth $\delta \ll L$) step illumination. At the end of the illumination there is

a measurable surface potential, termed the residual potential V_R , due to the bulk trapped charges. If positive charging is used, then V_R is due to trapped holes in the bulk of the specimen. The decay of surface potential, i.e., $V(t)$ versus t , during the illumination period is called the photoinduced-discharge characteristics (PIDC) of the photoconductor and has been extensively studied both theoretically and experimentally.³⁻⁶ The simplest theoretical model, based on range limitation and weak trapping ($V_R \ll V_0$), relates V_R to $\mu\tau'$ via the Warter equation⁷

$$V_R = L^2/2\mu\tau', \quad (1)$$

where L is the sample thickness. A more general description of the deep-trapping phenomenon during discharge involves solving the charge transport, continuity, detailed balance, and Gauss's equations within the material subject to appropriate boundary conditions. Kanazawa and Batra⁸ (KB), with certain assumptions, have solved the general equations and provided a universal curve⁹ that relates the normalized residual potential $v_R = V_R/V_0$ to the normalized trapping time $\tau = \tau'/t_0$, where t_0 is the transit time defined by $L^2/\mu V_0$. Their universal curve thus allows $\mu\tau'$ to be determined from the measurement of the residual potential at any charging voltage V_0 . In a different paper,¹⁰ Kanazawa and Batra also quote, without proof, an approximate implicit relationship between V_R and $\mu\tau'$ which, for weak trapping, is of the form,

$$V_R \approx (L^2/2\mu\tau')[-\ln(2V_R/V_0)]. \quad (2)$$

When compared with the Warter expression, Eq. (2) has the additional factor $[-\ln(2V_R/V_0)]$ which can be quite significant since $V_R \ll V_0$. It is apparent that an accurate $\mu\tau'$ determination from the residual potential must involve the KB universal curve since this is based on the most rigorous formulation of deep trapping during the discharge process. In Sec. II we will identify the problems associated with the various models, in particular the KB universal curve, currently used for $\mu\tau'$ product evaluations. In Sec. III, the KB model will be reformulated and a partial differential equation will be derived which describes correctly the space and time dependence of the electric field within the sample.

The time-of-flight (TOF) transient-photoconductivity (TP) technique is now widely used as a standard experimental method for studying charge transport in high-resistivity solids. Both the principle and the experimental requirements for TOF measurements have been extensively reviewed by numerous authors¹¹⁻¹⁷ who have also cited various applications of the technique to some specific materials. Recently it has gained further interest from the scientific community for characterizing charge transport in *a*-Si:H, chemically modified chalcogenides, and various polymeric materials. In general, the TOF measurement cannot be used directly to determine the charge-carrier lifetime τ' . When the carrier lifetime is less than the transit time, $t_0 = L^2/\mu V$, where V is the applied voltage, then the transport is range limited and the photocurrent decays rapidly without evincing a discernible transit time. When the lifetime, however, is much longer than the transit time, the observed photocurrent gives essentially no information on the carrier lifetime. The trapping-time measurements based on the conventional TOF technique generally rely on what is called the Hecht analysis.¹⁸ As the applied voltage is reduced the transit times become comparable to the deep-trapping time and the transport approaches the range-limited response regime. The carrier lifetime can then be determined via Hecht analysis of the TOF signal as demonstrated for various materials.¹⁹ Recent lifetime measurements on *a*-Si:H and *a*-Si:Ge:H have essentially employed a Hecht type of analysis.²⁰⁻²³ The latter technique becomes much more difficult and unreliable when the quantum efficiency is strongly field dependent, or when the applied field is comparable to any built-in field that might arise if *p-i-n* type of structures are used.

The transient-photoconductivity technique can still be used to determine the carrier lifetime by operating the TOF method in the interrupted field mode (or interrupted transit time mode) as demonstrated in Refs. 24-26. During the flight of the photoinjected carriers, at time $t = T_1$, the applied field is removed for a certain interruption time Δt and reapplied again at time $t = T_2$ to collect the remaining carriers. The fractional change I in the recovered photocurrent is related to the lifetime via

$$I = i_2/i_1 = i(T_2)/i(T_1) = \exp(-\Delta t/\tau'), \quad (3)$$

where $i(t)$ is the instantaneous photocurrent and τ' is the mean lifetime which represents the trapping effect of local-

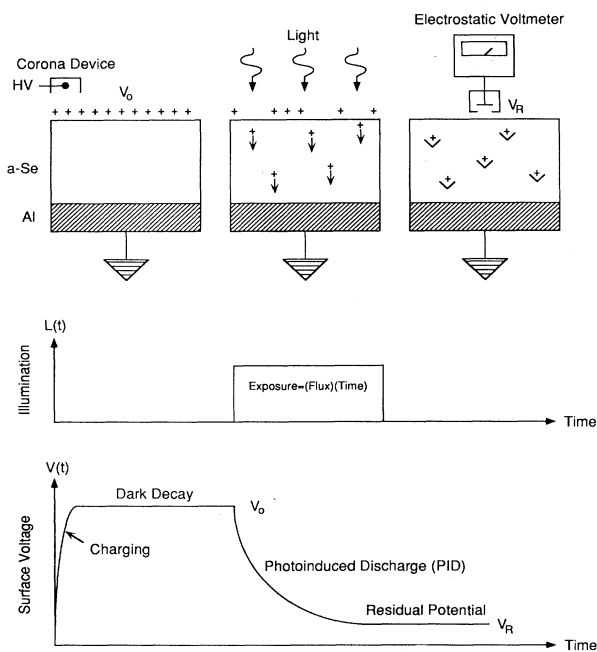


FIG. 1. A simple illustration of the xerographic experiment. The sample is first corona charged to a voltage V_0 and then exposed to step illumination. At the end of the illumination process, the remaining surface potential V_R is measured. PIDC is the photoinduced discharge characteristic of the photoinsulator.

ized states with release times τ_r , much longer than the interruption time; $\tau_r \gg \Delta t$. The interrupted-field TOF (IF-TOF) technique has a number of experimental difficulties but represents one meaningful way of studying charge-trapping kinematics.²⁷ Through Eq. (3), it allows the carrier lifetime to be readily determined. Its distinct advantages for charge-trapping studies have been only recently demonstrated by the present group.²⁸ In this work, the IFTOF technique is employed to evaluate the $\mu\tau'$ products of the *a*-Se and Cl-doped *a*-Se: 0.3 at. % As films used in xerographic experiments since it provides an independent and unambiguous determination of μ and τ' . Using the lifetime determined from the IFTOF technique, the residual potential is predicted from the deep-trapping kinematics model developed herein and compared with the experiments. Combined studied by IF-TOF and xerographic measurements are then used to evaluate the capture coefficient within the present models of charge trapping in amorphous semiconductors.

II. DEFICIENCIES OF PRESENT RESIDUAL POTENTIAL MODELS

It is instructive to bring to attention the deficiencies in the present theories relating to the residual potential to the $\mu\tau'$ product. The simplest relation derived by Warter, i.e., Eq. (1), has been recently found to predict the actual $\mu\tau'$ product remarkably well as checked by IFTOF measurements.²⁹ The agreement is in fact surprising inasmuch as the proof of Eq. (1) is based on range-limitation concepts and does not involve the formulation and solution of charge conduction, trapping, continuity and Gauss's equations in the material. It simply assumes that the charge per unit area on the surface, $\epsilon V_0/L$, is injected and a fraction, t_0/τ' or $L^2/\mu\tau'V_0$, of this becomes uniformly trapped in the bulk giving rise to the surface potential of Eq. (1). It has been recently used, for example, for determining $\mu\tau'$ in *a*-Si:H from the xerographic residual potential.³⁰

The theory of Kanazawa and Batra (KB) is based on solving the charge conduction, trapping rate, continuity, and Gauss's equations in the material subject to the appropriate boundary conditions. It is assumed that the rate of trapping is proportional to the concentration of deep traps and that the latter remains constant throughout the discharge process, i.e., deep-trap concentration N_t is much greater than the trapped-hole concentration p'_i at any point throughout the whole discharge process. The final result of their calculations is a universal curve relating the normalized residual potential $v_R = V_R/V_0$ to the normalized lifetime, $\tau = \tau'/t_0$, valid for any illumination profile as long as V_R is measured when the electric field at the surface is zero and it has reached steady state everywhere in the material. During the course of xerographic experiments, the present authors noticed that for a given $\mu\tau'$ product as determined from the IFTOF technique, the universal curve predicts residual potentials that are almost an order of magnitude higher than actual measured residual potential as well as that expected from the Warter equation. This discrepancy is also apparent in the literature. For example, Ab-

kowitz and Enck³¹ measure a residual of 1.8 V on a 48- μm -thick *a*-Se film charged to 200 V. The drift mobility and lifetime values for the same film were 0.16 $\text{cm}^2\text{V}^{-1}\text{s}^{-1}$ and 44 μs . With the latter values, the KB universal curve predicts a residual of 6.8 V, whereas the Warter equation gives 1.6 V in surprisingly good agreement with the experiment. Equation (2), on the other hand, gives 4.9 V. It should be mentioned that the present authors observed almost identical μ , τ' , and residual-potential values on a number of *a*-Se films in this laboratory. It is therefore clear that there is a need to identify the shortcomings of the KB model and reformulate the theory to properly account for the observed residuals. In this connection, one can immediately identify one major drawback of the KB analysis. According to the KB model, the final space-charge distribution in the sample is such that the top 30% of the specimen has a normalized charge density, $ep'_iL^2/\epsilon V_0$, of about ~ 1 when $\tau=1$, i.e., $\tau'=t_0$ (see Fig. 3 in Ref. 8). Thus the trapped-charge concentration in this case is given by

$$p'_i \approx \epsilon V_0 / eL^2 = \epsilon / e\mu\tau' = \epsilon C_t N_t / e\mu_0, \quad (4)$$

where trap controlled charge transport has been assumed so that $\mu\tau' = \mu_0\tau'_0 = \mu_0/C_t N_t$, μ_0 is the microscopic mobility, τ'_0 is the lifetime in the absence of shallow traps (i.e., $\tau'_0 = 1/C_t N_t$, and C_t is the capture coefficient. For the universal curve to be valid, the KB assumption of $p'_i \ll N_t$ must hold, which from Eq. (4), requires the following condition:

$$\epsilon C_t / e\mu_0 \ll 1. \quad (5)$$

From Eq. (5) it may be surmised that the assumption of negligible trap filling and thus the validity of the universal curve will be suspect when the microscopic mobility is small and/or the capture coefficient is large. This point will be critically examined in Sec. V.

In the next section, the discharge in the presence of shallow and deep traps will be reformulated to derive a more rigorous differential equation for the space and time dependence of the electric field.

III. DEEP-TRAPPING KINEMATICS IN XEROGRAPHIC EXPERIMENTS

To reformulate the KB model, it will be assumed that the photoconductor is positively charged and that electron-hole pairs are photogenerated very near the top surface. Holes are thus transported through the material toward the grounded substrate as illustrated in Fig. 2. During their transit across the film, holes are assumed to interact with a set of shallow traps at an energy ξ_s and become deeply trapped at localized states at an energy level ξ_d . Defining $p'(x',t')$ as the free-hole concentration in the transport band and $p'_{i1}(x',t')$, $p'_{i2}(x',t')$, as the trapped-hole concentrations at energy levels ξ_s and ξ_d at point x' at time t' , the following general equations thus hold.

(a) Conduction equation

$$J_c(x',t') = e\mu_0 p'(x',t') E'(x',t'), \quad (6)$$

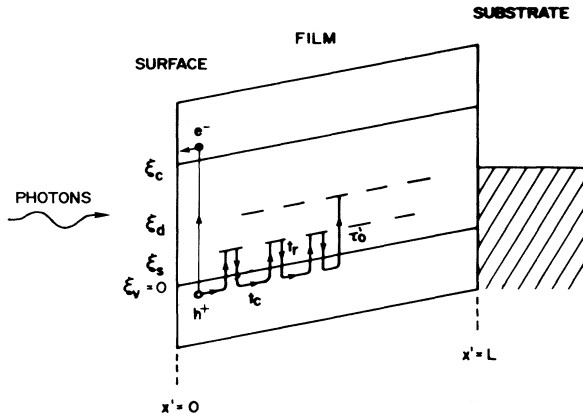


FIG. 2. Schematic energy-band diagram representing xerographic photodischarge process. The localized states at ξ_s and ξ_d correspond to shallow and deep traps, respectively. t_c and t_r are the capture and release times associated with ξ_s and τ_0 is the trapping time into ξ_d .

where $J_c(x', t')$ is the conduction current density, $E'(x', t')$ is the electric field, and μ_0 is the conductivity (microscopic) mobility.

(b) Maxwell's equation for the total current

$$J(t') = J_c(x', t') + \epsilon \partial E'(x', t') / \partial t', \quad (7)$$

where $\epsilon = \epsilon_r \epsilon_0$ is the permittivity of the medium.

(c) Gauss's equation in point form

$$\begin{aligned} \partial E'(x', t') / \partial x' = & (e / \epsilon) [p'(x', t') \\ & + p_{t1}(x', t') + p_t(x', t')]. \end{aligned} \quad (8)$$

(d) Continuity equation

$$\begin{aligned} \partial p'(x', t') / \partial t' = & -(1/e) \partial J_c(x', t') / \partial x' \\ & - \partial p_{t1}'(x', t') / \partial t' \end{aligned} \quad (9)$$

in which $\partial p_{t1}(x', t') / \partial t = 0$, i.e., traps at ξ_s are shallow.

(e) Rate equations without detrapping from ξ_d are

$$\partial p_t'(x', t') / \partial t' = p'(x', t') C_t [N_t - p_t'(x', t')], \quad (10)$$

$$\begin{aligned} \partial p_{t1}'(x', t') / \partial t' = & p'(x', t') / t_c - p_{t1}'(x', t') / t_r \\ = & 0, \end{aligned} \quad (11)$$

where N_t is the deep-trap concentration, C_t is the capture coefficient, t_c is the capture time into shallow traps, t_r is the release time from shallow traps, and $t_r \gg t_c$. The capture-to-release time ratio, t_c / t_r , is termed the shallow-trap-controlled reduction factor θ , and the quantity $1 / N_t C_t$ is the deep-trapping time denoted by τ_0' .

It is important to emphasize that Eq. (10) does not make the usual assumption of $N_t \gg p_t$ so that the second term can be neglected as in the KB formulation. In fact, this second term depends on the product of $p_t' p'$ and thus makes the rate equation nonlinear with the result that it

couple the space and time derivatives of $E'(x, t)$ as shown below. It has a profound effect on the final electric-field distribution within the material.

In the above equations $J_c(x', t')$ is the conduction current whereas $J(t')$ is the total current which in the xerographic experiments is zero; the surface potential is monitored with the sample grounded at one end only (Fig. 1). Thus the result of xerographic experiments is the instantaneous space integral of the electric field across the sample whereas, in contrast, in time-of-flight transient-photoconductivity experiments the total current $J(t)$ is monitored.

It is convenient to convert the above equations to dimensionless variables by defining

$$x = x' / L, \quad (12a)$$

$$t = t' / t_0, \quad (12b)$$

$$p(x, t) = e L p'(x', t') / C V_0, \quad (13a)$$

$$p_{t1}(x, t) = e L p_{t1}'(x', t') / C V_0, \quad (13b)$$

$$p_t(x, t) = e L p_t'(x', t') / C V_0, \quad (13c)$$

$$E(x, t) = E'(x', t') / E'_0, \quad E'_0 = V_0 / L, \quad (14)$$

$$j_c(x, t) = t_0 J_c(x', t') / C V_0, \quad (15)$$

$$\tau = \tau' / t_0, \quad (16a)$$

$$\tau' = \tau_0' / \theta = 1 / (\theta N_t C_t), \quad (16b)$$

$$\tau_0' = 1 / C_t N_t, \quad (16c)$$

and

$$c = \epsilon C_t / e \mu_0 = \epsilon \theta C_t / e \mu, \quad (17)$$

where $\mu = \theta \mu_0$ is the shallow-trap-controlled drift mobility, $t_0 = L / \mu E'_0$ is the transit time, $E'_0 = V_0 / L$ is the initial field, $C = \epsilon / L$ is the capacitance per unit area, and V_0 is the initial voltage. The quantities τ and c represent *normalized shallow-trap-controlled* lifetime and capture coefficient.

Equations (6)–(10) can now be recast into dimensionless forms

$$\theta j_c(x, t) = p(x, t) E(x, t), \quad (18)$$

$$j_c(x, t) + \partial E(x, t) / \partial t = 0, \quad (19)$$

$$\partial E(x, t) / \partial x = p(x, t) + p_t(x, t) + p_{t1}, \quad (20)$$

$$\partial p(x, t) / \partial t = -\partial j_c(x, t) / \partial x - \partial p_t(x, t) / \partial t, \quad (21)$$

$$\theta \partial p_t(x, t) / \partial t = p(x, t) / \tau - c p(x, t) p_t(x, t), \quad (22)$$

$$p(x, t) = \theta p_{t1}(x, t). \quad (23)$$

Clearly, c is the coefficient of the cross-product term since it appears in $p p_t$. It couples $\partial E / \partial x$ with $\partial E / \partial t$ via Eqs. (18)–(20) and thus serves as a coupling factor in the final differential equation. By eliminating $p(x, t)$, $p_t(x, t)$, $p_{t1}(x, t)$, and $j_c(x, t)$ in Eqs. (18)–(23), it is not difficult to derive a partial differential equation for $E(x, t)$ only. The result is a nonlinear second-order partial differential equation that describes the variation of the electric field

as a function of x and t , viz.,

$$E(\partial^2 E / \partial t^2) + E^2(\partial^2 E / \partial x \partial t) - (1+c)(\partial E / \partial t)^2 - c(\partial E / \partial x)(\partial E / \partial t) + (1/\tau)E(\partial E / \partial t) = 0. \quad (24)$$

In deriving Eq. (24) we made the usual assumption that $\theta \ll 1$. Equation (24) is the partial differential equation that describes not only the PIDC, inasmuch as it is applicable at all times, but also the final electric field in the sample when the surface charge has been depleted by photoinjection. It should be remarked that in the presence of shallow traps the effective capture cross section and mobilities are θC_i and $\theta \mu_0$ so that the measured lifetime τ' is enhanced with respect to the shallow-trap free lifetime τ'_0 by $1/\theta$. Note also that τ' is defined as the effective lifetime in the trapped space-charge free material, i.e., before the photodischarge. Although, a discrete manifold of shallow traps was employed in the development of the theory, a distribution of shallow traps up to some energy ξ_s from the valence band will essentially have the same effect provided that the longest release time t_r from the shallow traps is such that it is much shorter than the transit time, i.e., $t_r \ll t_0$. Thus, in the presence of a shallow distribution of localized states described by a density of states, $N(\xi)$, the shallow-trap reduction factor θ is given by

$$1/\theta = \int_0^{\xi_s} [N(\xi)/N_v] \exp(\xi/kT) d\xi \quad (25)$$

which essentially introduces only a temperature-dependent numerical factor into transport and trapping parameters, μ and τ' .

The solution of Eq. (24) subject to the appropriate boundary conditions will give the electric field at position x at time t . Equation (24) with $c=0$ reduces to that derived by Okuda *et al.*³² when release from deep traps is neglected. If the electric field at the surface is zero at time $t=t_1$, then the normalized residual potential $v_R = V_R/V_0$ is given by

$$v_R = \int_0^1 E(x, t_1) dx. \quad (26)$$

The necessary boundary conditions imposed by the experimental conditions in the present case are

$$p(x, 0) = 0, \quad (27a)$$

$$p_t(x, 0) = 0, \quad (27b)$$

$$E(x, 0) = 1. \quad (27c)$$

Furthermore, the current $j_c(0, t)$ is proportional to the quantum efficiency η , which in turn depends on the electric field so that it is appropriate to write $j_c(0, t) = KE(0, t)^m$, where K is a constant that includes the illumination intensity and m is an index defining the electric field dependence of η , i.e., $\eta \sim E(0, t)^m$. The flux dependence of the quantum efficiency is neglected in this work. Thus, at the surface, at any time,

$$E(0, t) = [1 - (1-m)Kt]^{1/(1-m)}, \quad m \neq 1 \quad (28a)$$

$$E(0, t) = \exp(-Kt), \quad m = 1. \quad (28b)$$

For the present calculations, it is assumed that $m = \frac{1}{2}$

so that the electric field at the surface vanishes at a well-defined time, i.e., when $t=t_1=2K$. Moreover, $m = \frac{1}{2}$ is also a reasonable index for the electric field dependence of η . Note that $m=0$ is tantamount to a field-independent quantum efficiency which is not generally the case. If the residual potential is measured when $E(0, t)=0$, say in practice at time $t'=2$ sec, then $K=10^{-6}$ which is also the value used by Kanazawa and Batra. With the above boundary conditions, the partial differential equation (24) can be solved numerically to obtain $E(x, t_1)$ and hence v_R . In this work, Eq. (24) was solved numerically subject to the above boundary conditions by using Taylor expansions for the derivatives. The results from the numerical solution of Eq. (24) will be presented along with the experimental results in Sec. V.

IV. EXPERIMENTAL PROCEDURE

The general experimental procedure for xerographic measurements have been previously described by various authors.^{6,30,31,33-35} The present xerographic measurement system uses an aluminum turntable to pass the sample through various xerographic steps as shown schematically in Fig. 3. The sample was charged at position *A* by passing it under a scorotron.³⁶ The surface potential was then measured at station *B* by a Monroe electrovoltmeter probe type 1009B connected to an electrovoltmeter type 144S-4. The output of the Monroe electrostatic voltmeter was interfaced, via a 12 bit A/D autoranging converter, to an IBM-compatible microcomputer for data acquisition, analysis, display, and storage. Following charging, the sample could be exposed to either a xenon flash at *C* or step illumination at *D*. The xenon flash exposure could be either single shot or repetitive up to 100 Hz. Its output was passed through a 445-nm filter (bandwidth 60 nm). A halogen light source with a blue filter centered at 450 nm (bandwidth ~ 150 nm) was used for the step illumination. The output density from both the xenon flash and the halogen lamp was user adjustable. The photon flux arriving at the sample surface was determined by using a calibrated Si photodiode. Following exposure, the residual potential was measured at position *E* by a second Monroe electrostatic voltmeter. The turntable could be stopped at any point for any duration, for the sample to be charged, exposed to illumination, or to have its surface potential measured. Timing sequences and periods were conveniently generated by using reed relays and IC timers. Exposure, viz., (flux) \times (exposure time), could be readily varied by either adjusting the flux or the exposure time. The latter was controlled by an electronic shutter.

Interrupted-field time-of-flight measurements were carried out as described previously^{28,29} by using a Schering-type bridge network, illustrated in Fig. 4, to eliminate the large transient voltages occurring at the switching on and off times of the applied voltage. With the present apparatus, using a totem-pole configuration of TMOS transistors for switching, bias voltages up to 1 kV could be interrupted so that the *a*-Se samples of xerographic thickness could be readily examined.³⁷ The IFTOF measurement was carried out under a single-shot mode of

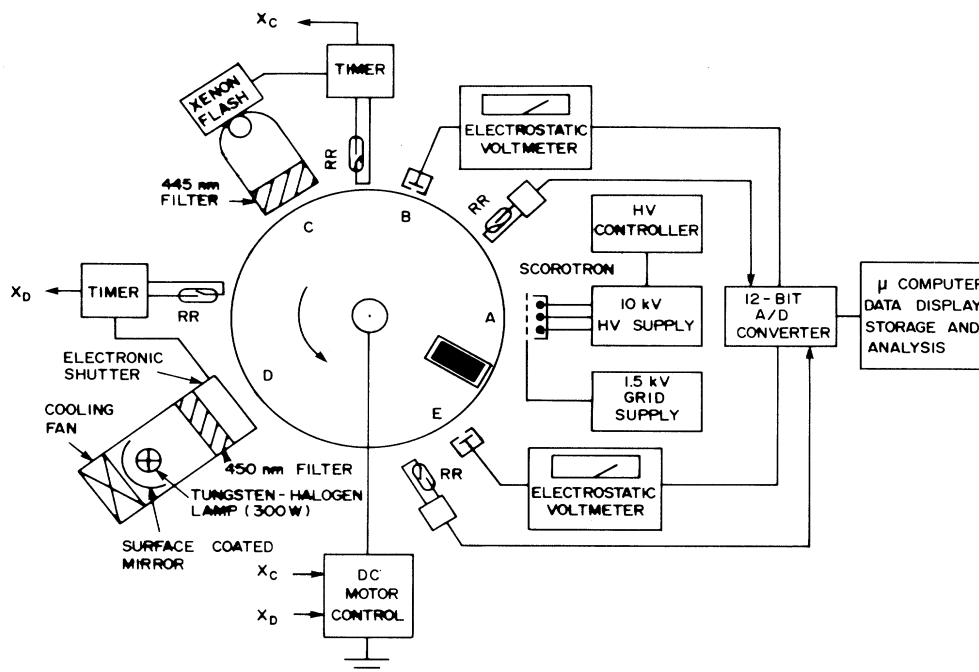


FIG. 3. A schematic diagram of the xerographic experiment.

operation and between each measurements the sample was short circuited and rested in the dark for any bulk space-charge buildup to decay. Small signal conditions were maintained throughout all the measurements.

The α -Se films were prepared by conventional vacuum evaporation techniques as described previously.³⁸ Vitreous selenium pellets, obtained from Noranda Technology

Centre, Pointe Claire, Quebec, were evaporated from a directly heated Mo boat onto preoxidized Al plates held at various substrate temperatures. By deliberately varying the preparation conditions, e.g., the substrate temperature, or using different batch vitreous selenium pellets, the deposited films could be made to exhibit hole lifetimes varying over an order of magnitude. The variation of

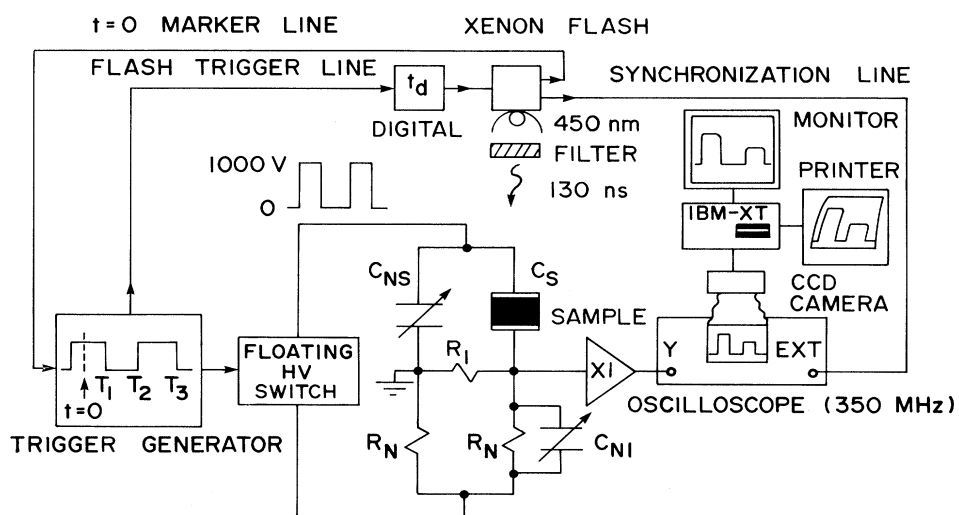


FIG. 4. A schematic diagram of the interrupted-field time-of-flight transient-photoconductivity apparatus.

hole lifetime from batch to batch, or as a result of preparation conditions, is well documented.³⁹ A small number of Cl-doped *a*-Se:0.3 at. % As films were also prepared by vacuum deposition so that a wider range of hole lifetimes could be accessed in the xerographic and IFTOF measurements. From the literature, it is known that combinational doping of *a*-Se by 0.3–0.5 at. % As and 10–20 ppm Cl extends the hole range.^{40,41} The bulk As content of the films were obtained by scanning electron microprobe analysis. Following deposition, the Al substrate was cut into two pieces to provide two identical *a*-Se samples for xerographic and IFTOF measurements. For the latter, a semitransparent Au electrode was sputtered onto the surface of the specimen. Since one of the films goes through an electrode deposition process, the two films are not expected to be identical as far as structural defects are concerned. The films were then heated to about 35 °C for 2 h, returned to room temperature, and annealed for several days. This identical thermal treatment is expected to make the two films contain similar concentration of structural defects. Amorphous Se is an ideal prototype material for the present study because after prolonged annealing at room temperature, its structure is in its well-relaxed state thus reducing the thermal hysteresis effects on the measured properties.^{42–46}

V. EXPERIMENTAL RESULTS AND DISCUSSION

Figures 5(a) and 5(b) displays typical conventional and IFTOF hole photocurrent waveforms obtained on a Cl-doped *a*-Se:0.3 at. % As film at a bias voltage of 1 kV where it can be seen that, although the conventional TOF signal indicates essentially negligible trapping over the transit time, in the IFTOF mode, the recovered signal is clearly affected by deep trapping. Figure 6 shows a semi-

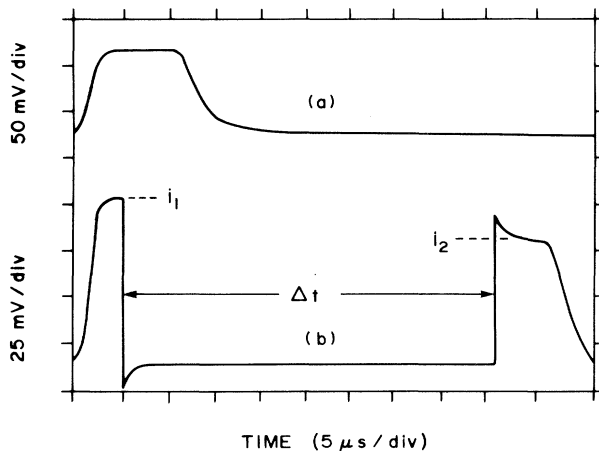


FIG. 5. (a) Conventional TOF hole photocurrent at a bias voltage of 1000 V. (b) The photocurrent in (a) is interrupted for a duration of $\Delta t = 40 \mu\text{s}$. The interruption voltage is 1000 V as in (a) whereas the photosignal is only about 80 mV.

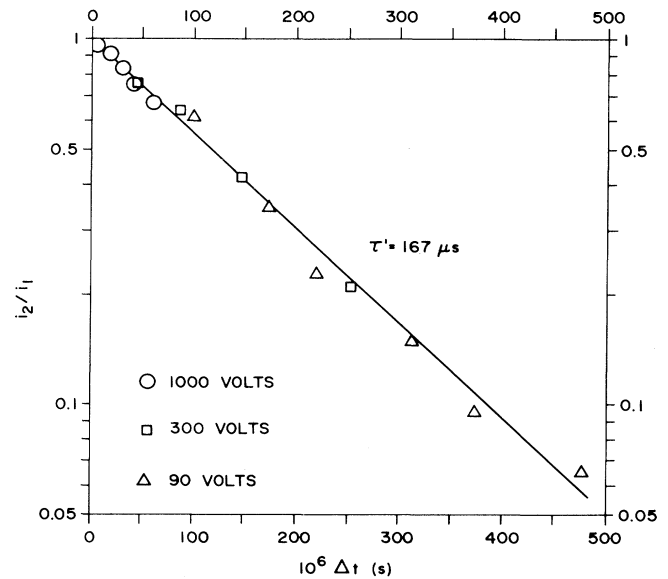


FIG. 6. Semilogarithmic plot of the fractional recovered photocurrent vs interruption time at various applied (interruption) voltages.

logarithmic plot of the fractional recovered photocurrent against the interruption period at various bias voltages. It should be noticed that the recovered photocurrent decays exponentially, following Eq. (3), with a well-defined hole lifetime τ' up to times extending to 500 μs , at least an order of magnitude beyond typical transit times. It should be mentioned that an exponentially decaying photocurrent behavior could only be observed under a low-level injection condition on well and dark rested specimens which were free of any bulk space charge. If the samples were preilluminated even with weak white light, or space charge was allowed to buildup during the measurements by insufficient resting between IFTOF measurements, the observed decay in the recovered photocurrent deviated from the well-defined exponential behavior and resembled $I \sim t^{-n}$ type of decay for times in excess of the transit time as reported in a previous paper.⁴⁷ Interruption of the photocurrent at different locations within the sample showed that in bulk space-charge free specimens, the hole lifetime was uniform across the specimen thickness as demonstrated previously.²⁸ We believe that the lifetime determinations from the exponential decay of the fractional recovered photocurrent reflect the true trapping behavior of the photoinjected holes. As a further check, for those samples exhibiting considerable trapping, hole lifetime determined from the shape of the photocurrent under a low bias voltage (long transit times) was found to be approximately the same as that from the IFTOF measurement at high applied voltages. In addition, it was observed that the examination of the fractional charge collected, i.e., integration of the photocurrent, instead of the recovered fractional photocurrent, resulted in almost identical lifetime values. Using IFTOF mea-

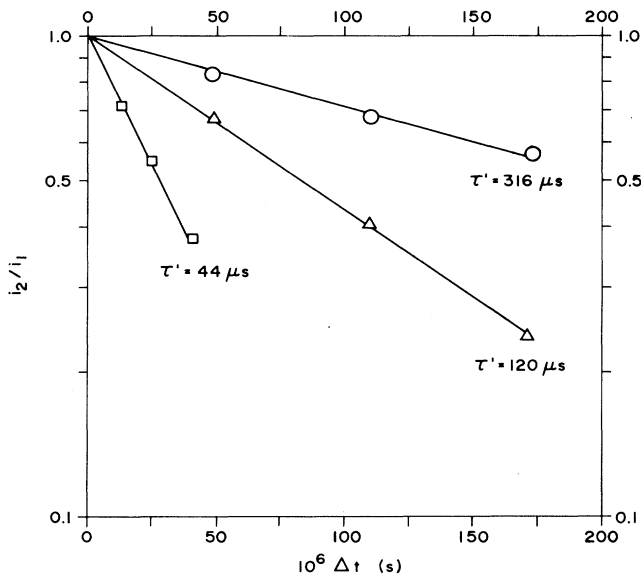


FIG. 7. Typical semilogarithmic plots of the fractional recovered photocurrent vs interruption time for three different samples with different hole lifetimes. Δ and \square are pure α -Se whereas \circ is chlorinated and 0.3 at. % AS alloyed α -Se.

measurements, μ and τ' were determined for all the specimens examined in xerographic experiments. It is instructive to remark that the hole lifetime in Fig. 6 is at zero-applied-field conditions. Figure 7 shows typical IFTOF results on various α -Se and Cl-doped α -Se:0.3 at. % As

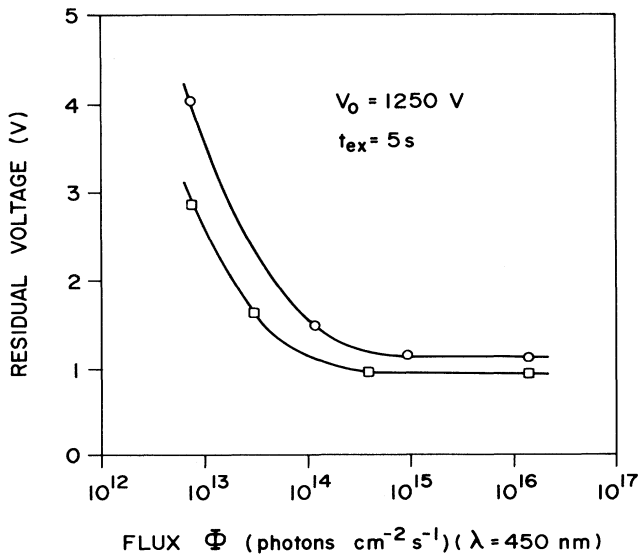


FIG. 8. First-cycle xerographic residual potential vs illumination flux (photons $\text{cm}^{-2} \text{s}^{-1}$). The illumination center wavelength was 450 nm and the exposure time was 5 s.

films where it can be seen that the hole lifetime depends on the sample material.

With the samples charged to several hundred volts, upon exposure it was found that the residual potential was typically a few volts, usually in the range 1–10 V. The specimens studied, therefore, exhibited weak trapping ($V_R \ll V_0$). It was observed that provided the exposure flux was sufficiently large, V_R , was insensitive to the light intensity but showed some dependence on the charging voltage. Figure 8 displays the dependence of the residual potential V_R on the light flux Φ at a constant charging voltage, where it can be seen that at the highest light intensities V_R reaches a constant value independent of the flux. Furthermore, it was found that photoinduced discharge by repetitive xenon flash exposure resulted in almost the same V_R values within experimental errors. The dependence of the residual potential on the exposure time t_{ex} is shown in Fig. 9 under a constant high-intensity step illumination. It can be seen that V_R is independent of the exposure time which implies that under strong illumination V_R is independent of the light exposure, (Φt_{ex}). Moreover, over a time scale up to the longest exposure time of 5 sec, the release of trapped holes is negligible. These experimental observations are in agreement with the general predictions of the KB theory that the final residual potential should be independent of the light intensity provided the surface charge has been dissipated and the electric field has reached steady state in the sample. Figure 10 shows the dependence of the residual potential on the charging voltage under a constant light-flux exposure (corresponding to a constant V_R at a given V_0 in Fig. 8). It can be seen that V_R increases with V_0 as qualitatively expected from the KB model. Figure 10 also shows the expected residual potentials from the universal curve, Eq. (2), and the Warter equation using as input lifetime values from IFTOF measurements. It is apparent that the experimental points are surprisingly

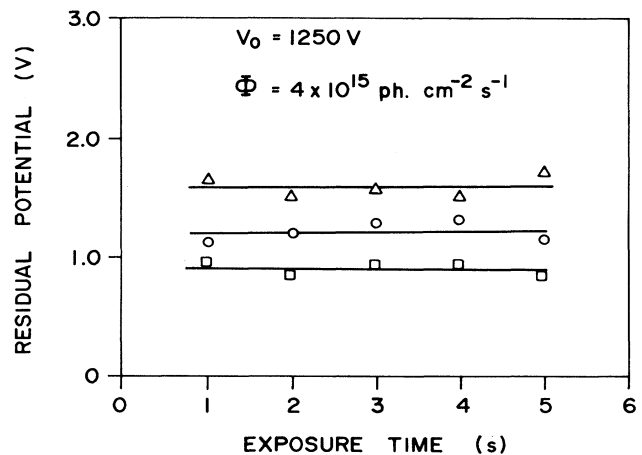


FIG. 9. First-cycle residual potential vs exposure time at a fixed photon flux and identical initial charging voltages.

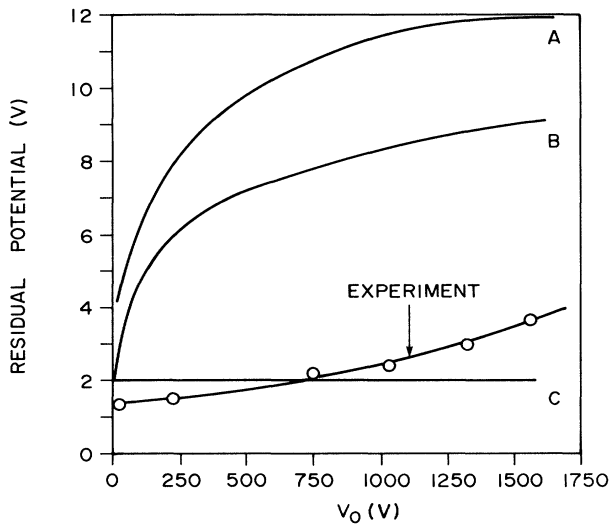


FIG. 10. First-cycle xerographic residual potential (V_R) vs initial voltage (V_0) photodischarged by a constant light flux ($\sim 10^{16}$ photons cm^{-2} , s^{-1} ; exposure time is 5 s). *A* is the KB universal curve (Fig. 3 in Ref. 8), *B* is the KB weak-trapping equation whereas *C* is the Warter expression, $V_R = L^2/2\mu\tau'$.

close to the Warter equation whereas the universal curve overestimates the residual potential by a factor of 5. The inadequacy of the present residual potential models is quite obvious from this figure.

The solution of the partial differential equation (24) for $E(x,t)$ when the field at the surface reaches zero, i.e., at $t'=2$ s, is shown in Fig. 11 for various values of the normalized capture coefficient c from 0 to 10. It can be seen that although when $c=0$, $E(x,t)$ is practically identical to that expected from the KB theory, when $c>0$, the electric field is lower than the $c=0$ case and decreases with c . Thus the residual potential corresponding to $c>0$ will also be lower. Another noticeable feature is that the electric field profiles becomes almost linear as c increases, indicating that the trapped space-charge distribution, proportional to $\partial E/\partial x$, becomes more uniform across the specimen with larger c . Indeed, the $c=1$ case coincides, probably fortuitously, with the Warter case in which the field is linear across the sample. The electric fields in Fig. 11 can be integrated to obtain the normalized residual potential v_R as a function of τ for various values of c as shown in Fig. 12, where v_R is plotted against τ for $c=0$ to 10. The $c=0$ case corresponds to the universal curve of KB. The most important feature of the v_R versus τ curves in Fig. 12 is that as c increases

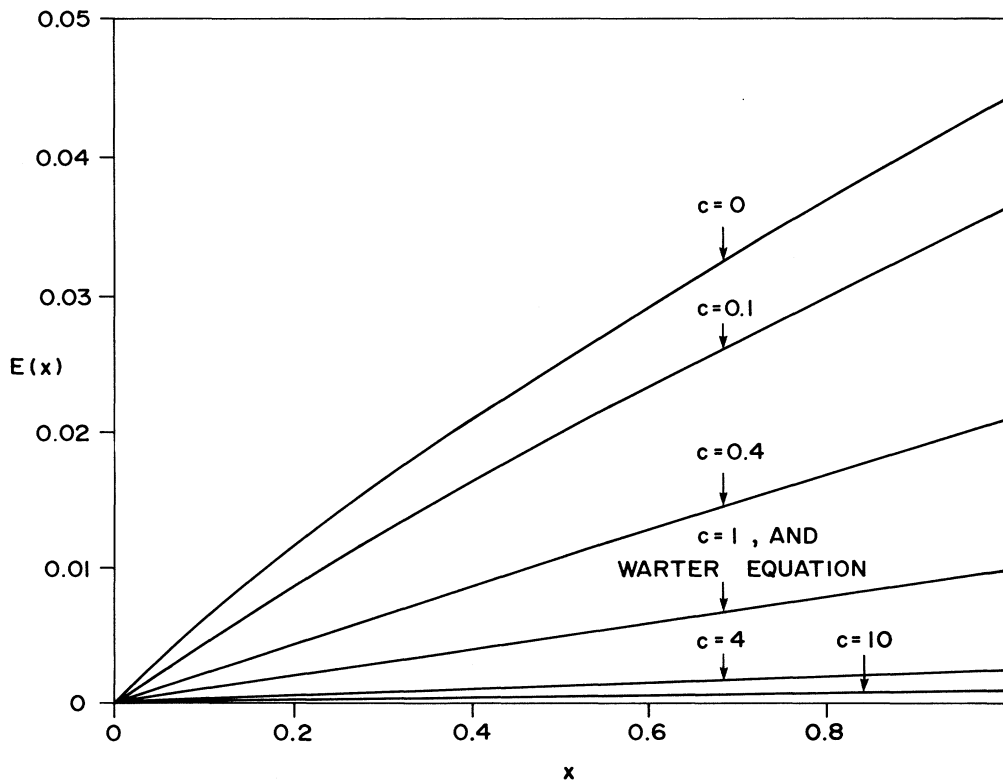


FIG. 11. The normalized electric-field profiles, $E(x,t)$, in the sample at the end of the illumination (photogeneration) process for various values of the normalized capture coefficient $c = \epsilon C_i / \epsilon \mu_0$. The electric field in the Warter model is linear and coincides with $c=1$. The electric field for $c=0$ is identical to that predicted by KB analytical treatment.

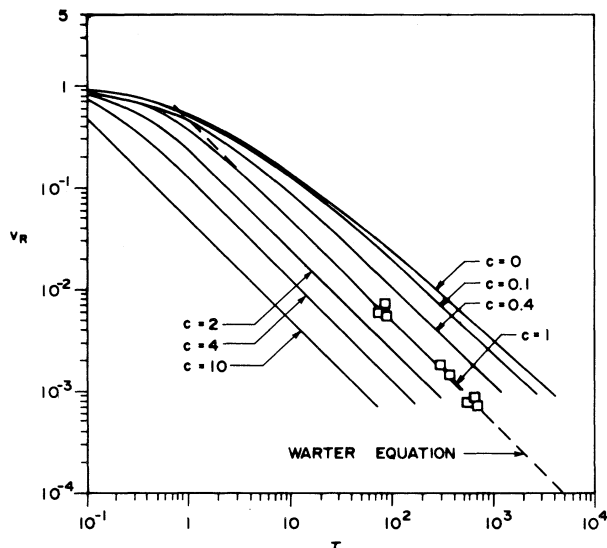


FIG. 12. "Universal curves" parametric in c resulting from the numerical solutions to Eq. (24). The $c=0$ case is the KB universal curve (Fig. 3 in Ref. 8). The combined results from IFTOF hole lifetime and xerographic residual potential measurements on a range of a -Se samples are plotted as experimental points and fall close to the $c=1$ line.

they shift downwards to lower residual potential values. It is clear that a residual potential measurement at one charging voltage, or indeed at a series of charging voltages, i.e., V_R versus V_0 , cannot be used to uniquely determine the $\mu\tau'$ product. The latter finding is contrary to the general consensus in the literature that $\mu\tau'$ can be readily determined via simple xerographic measurements. We therefore find, strictly, a single xerographic measurement in general cannot be used to accurately determine the $\mu\tau'$ product, unless $c \ll 1$.

Using lifetime values determined from IFTOF measurements, it is possible to plot v_R versus τ from combined first-cycle xerographic and IFTOF experiments as indicated in Fig. 12, where each point corresponds to a different a -Se sample. The immediate observation is that all the experimental v_R versus τ values fall around the $c=1$ curve and hence imply that the lifetime variations from sample to sample cannot be due to changes in the capture process and thus must be due to the variations in the integrated density of deep traps. Figure 13 shows typical v_R versus τ points obtained by varying the charging voltage on a given a -Se film. Again, the experimental values fall close to the $c=1$ curve and the Warter line.

Typical results from the cycled-up xerographic measurements are displayed in Fig. 14 for two a -Se samples and one chlorinated a -Se:0.3 at. % As sample, with different IFTOF lifetime values, where it can be seen that the larger the first-cycle residual, V_{R1} , the higher is the saturated residual potential $V_{R\infty}$. The saturated value $V_{R\infty}$ corresponds to all the deep traps in the bulk being filled and occurs typically after ~ 100 xerographic cycles.

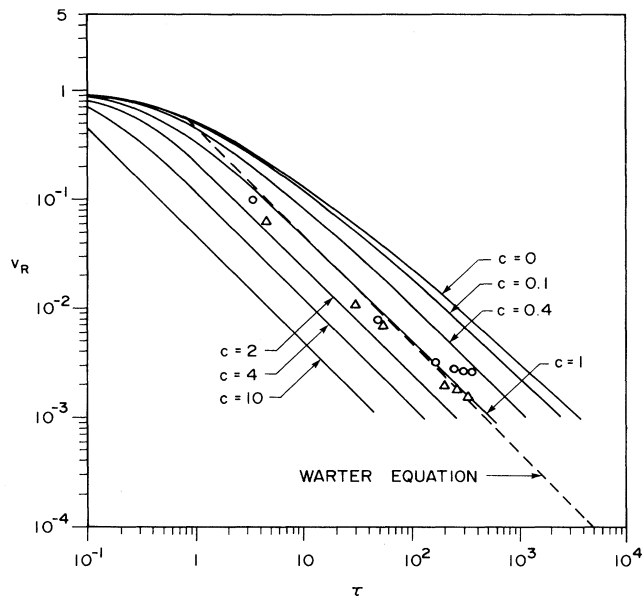


FIG. 13. Normalized residual potential vs normalized lifetime data on two a -Se samples obtained by varying the charging voltage. Lifetime data were obtained from IFTOF measurements on the same samples.

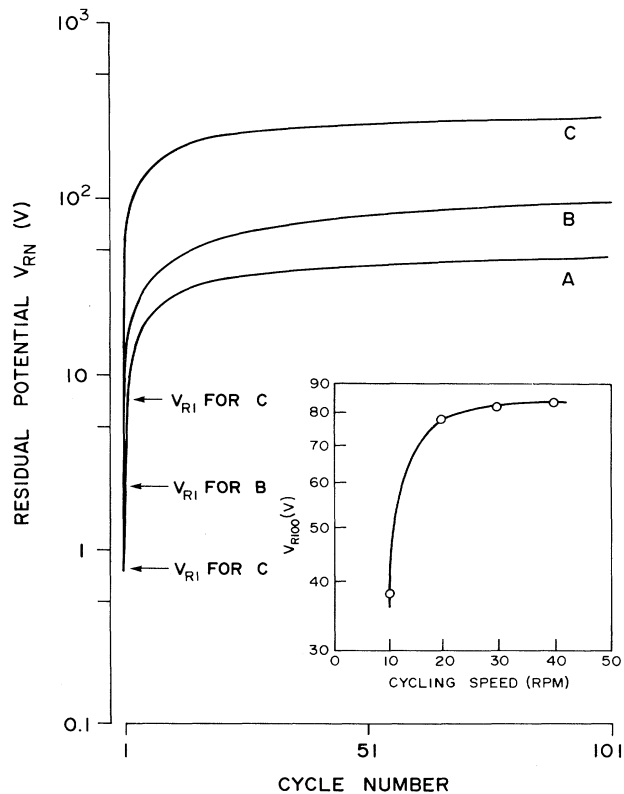


FIG. 14. Typical cycled-up xerographic experiments on two a -Se (A and B) and one chlorinated 0.3 at. % alloyed a -Se (C) films. The first-cycle residual potentials are identified. The inset shows the dependence of the residual potential at the 100th cycle on the cycling speed; V_{RN} vs dN/dt .

The trap-filling interpretation can be readily verified by checking whether $V_{R\infty}$ shows any dependence on the cycling frequency to exclude a dynamic equilibrium condition involving trap filling and emptying as illustrated in the lower inset of Fig. 14. The saturated residual potential is then simply given by

$$V_{R\infty} = eN_t L^2 / 2\epsilon_0 \epsilon_r, \quad (29)$$

where N_t is the deep-trap concentration. The results from the saturated residual potential can be used in conjunction with IFTOF lifetime values to evaluate the capture radius of the traps. For ballistic capture of carriers from the mobility edge, Street derives⁴⁸

$$\pi r_b^2 = (ea/6kT)(\mu\tau'N_t)^{-1}, \quad (30)$$

where r_b is the ballistic capture radius and a is the scattering length at the mobility edge. For diffusional capture, viz., mean free path much smaller than the capture radius, using the Waite formulation,⁴⁹ Street obtains⁴⁸

$$r_d = (e/4\pi kT)(\mu\tau'N_t)^{-1}, \quad (31)$$

where r_d is the diffusional capture radius. IFTOF and cycled-up xerographic experiments essentially give $\mu\tau'$ and N_t so that substituting for N_t and rearranging,

$$1/\mu\tau' = (12\pi r_b^2 \epsilon_0 \epsilon_r kT / e^2 a) (V_{R\infty} / L^2) \quad (32)$$

for the ballistic case, and

$$1/\mu\tau' = (8\pi r_d \epsilon_0 \epsilon_r kT / e^2) (V_{R\infty} / L^2) \quad (33)$$

for the diffusional case. It should be noticed that the evaluation of the capture radius from the measured $\mu\tau'$ product does not depend on μ_0 within the two models considered. Both r_b and r_d can be readily determined via the slope of $1/\mu\tau'$ versus $V_{R\infty}/L^2$ plot as shown recently.²⁹ Figure 15 shows the dependence of $1/\mu\tau'$ on V_{R100}/L^2 for the various pure *a*-Se and chlorinated *a*-Se:0.3 at. % As samples investigated in this work. It can be seen that the data imply that $\mu\tau'$ variations from sample to sample in *a*-Se are essentially due to variations in the integrated deep-trap concentration rather than the capture cross section. Furthermore, the deep-hole capture process in Cl-doped and 0.3 at. % As alloyed *a*-Se is the same as that in pure *a*-Se but with a much lower integrated density.

Table I summarizes the capture radii calculated via Eqs.(32) and (33) and the slope from Fig. 15. In the ballistic case, the capture radius calculation depends on the value assumed for the scattering length a . For

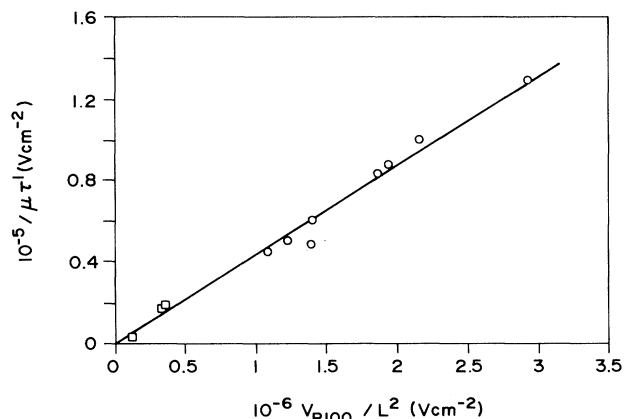


FIG. 15. Reciprocal $\mu\tau'$ vs $V_{R\infty}/L^2$ plot of the IFTOF $\mu\tau'$ and the saturated residual voltage $V_{R\infty}$ data. \circ refer to *a*-Se whereas \square refer to 10–20-ppm Cl-doped 0.3 at. % As alloyed *a*-Se films.

$a = 5-10 \text{ \AA}$, r_b is $2.5-3.5 \text{ \AA}$. The diffusional capture radius, on the other hand, was determined to be 1.9 \AA . For comparison purposes, the table also shows the various capture radii in *a*-Si:H. It is instructive to mention that if one uses a thermal velocity $v_{th} = 10^7 \text{ cm s}^{-1}$ as in charge transport in crystalline materials, the capture cross section is then given by

$$\pi r_c^2 = \mu_0 / (\mu\tau' v_{th} N_t), \quad (34)$$

which with $\mu_0 = 0.44 \text{ cm}^2 \text{ V}^{-1} \text{ s}^{-1}$ from Abkowitz and Pai⁵⁰ predicts an r_c of about 1 \AA . The latter value is too small to represent trapping into a charged center, implying that either the estimate for μ_0 is too small or the mean velocity of holes is much less than v_{th} .

The energy distribution of the deep localized states and its variation from sample to sample can be readily studied via the xerographic-spectroscopy technique of Abkowitz and Markovics⁵¹ which simply monitors the rate of decay of the residual potential at the end of the cycled-up experiments. Figure 16 shows typical residual voltage decay curves normalized with respect to the cycled-up saturated residual potential for *a*-Se and chlorinated *a*-Se:0.3 at. % As samples. Notice that the decay of the residual potential occurs over a longer period of time for the Cl-doped 0.3 at. % As alloyed *a*-Se films.

The xerographic-spectroscopy method assumes that at

TABLE I. Deep-trap capture radii.

Material/Trapping	Ballistic (\AA)	Diffusional (\AA)	Measurement method
<i>a</i> -Se, h^+ trapping	2.5–3.5 ($a = 5-10 \text{ \AA}$)	1.9	IFTOF $\mu\tau$ and cycled-up residual $V_{R\infty}$
<i>a</i> -Se, h^+ trapping	17–24 ($a = 5-10 \text{ \AA}$)	85	IFTOF $\mu\tau$, V_{R1} , and universal curves
<i>a</i> -Si:H, $e^- \rightarrow D^0$	2.9 ($a = 10 \text{ \AA}$)	1.3	TOF Hecht analysis by Street
<i>a</i> -Si:H, $h^+ \rightarrow D^0$	5.0 ($a = 5 \text{ \AA}$)	4.8	TOF Hecht analysis by Street

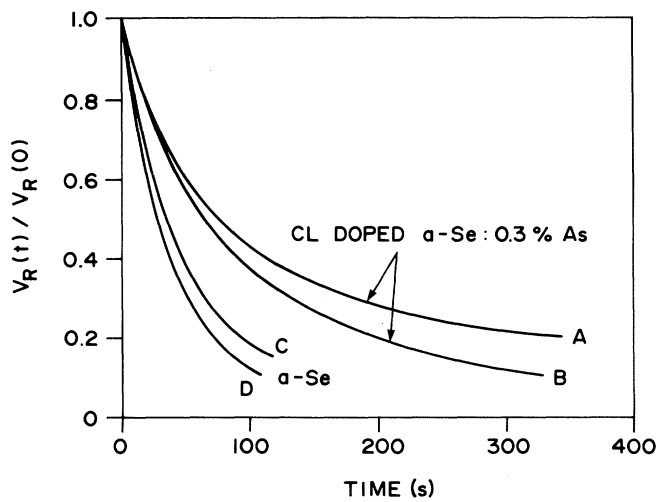


FIG. 16. The decay of the saturated residual potential following the end of cycled-up xerographic experiments. The instantaneous residual voltage data are normalized to the saturated ($V_{R\infty}$) value. *A* and *B* are chlorinated and 0.3 at. % alloyed *a*-Se, whereas *C* and *D* are pure *a*-Se films.

time t , the emission essentially occurs from a narrow band of energies around $\xi = kT \ln(\nu T)$ so that the density of states $N(\xi)$ is⁵¹

$$N(\xi) = (2\epsilon / eL^2 kT) t |dV/dt|, \quad (35)$$

where dV/dt is the slope of the residual potential versus time characteristic. Equation (35) was in fact derived by Abkowitz and Markovics by applying Simmon's formula-

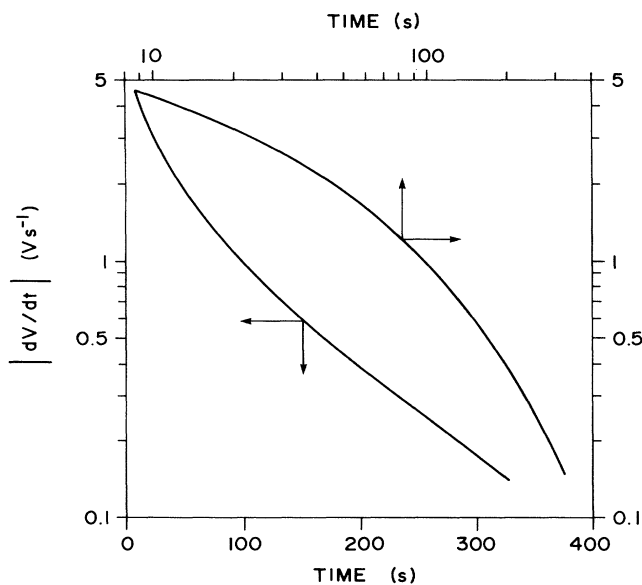


FIG. 17. Semilogarithmic and log-log plots of the magnitude of rate of discharge against time.

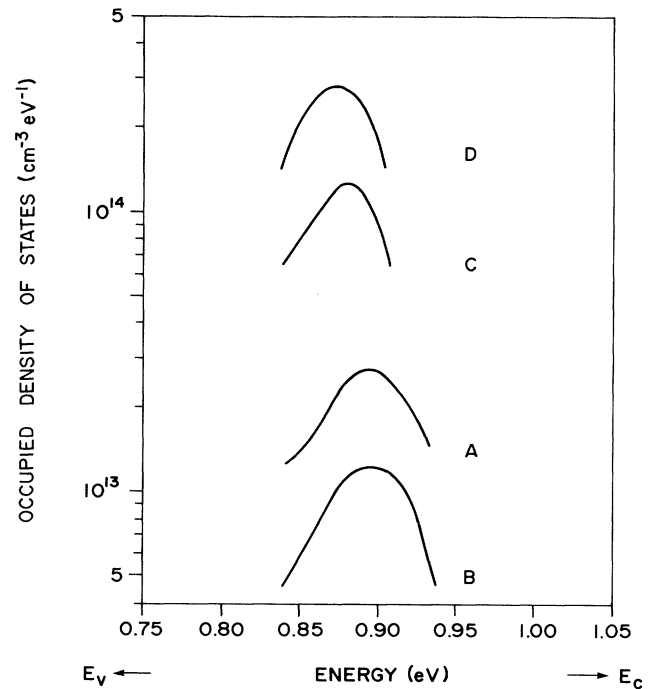


FIG. 18. Density of states vs energy from xerographic-spectroscopy experiments (from Fig. 16) for pure *a*-Se and chlorinated and 0.3 at. % As alloyed *a*-Se films. The labels *A*–*D* refer to the same samples as those used in Fig. 16.

tion of charge-emission kinetics from an arbitrary distribution of localized states^{52–54} to the xerographic case in which the residual decay is due to the emission of trapped holes. Application of Eq. (35) to the present residual potential data is therefore subject to the limitations discussed by Simmons and Tam⁵⁴ and Naito *et al.*⁵⁵ Figure 17 shows a semilogarithmic and log-log plots of the decay of the residual potential on a typical Cl-doped *a*-Se:0.3 at. % As film. It can be seen that neither a simple exponential nor a power-law time dependence can account for the dark discharge. The former would result for emission from a single discrete trap level whereas the latter for emission from an exponential distribution of localized states. Figure 18 displays typical density-of-states functions obtained by applying Eq. (35) to the data in Fig. 16 for two *a*-Se and two Cl-doped 0.3 at. % As alloyed *a*-Se samples with different IFTOF lifetime values. It was found that from sample to sample the peak of the distribution for pure *a*-Se remained very close to 0.87 eV in agreement with the previous measurements⁵¹ but the peak density varied from sample to sample. For the chlorinated *a*-Se:0.3 at. % As films, the peak was located at almost 0.9 eV but with a peak density which was considerably smaller than that for pure *a*-Se. Thus, chemical modification of *a*-Se with Cl doping and 0.3 at. % As alloying results in a drastic reduction of the integrated deep-trap density which is a technological advantage.

VI. DETAILED DISCUSSION

Taking $c \approx 1$ as an approximate result of the xerographic residual potential measurements with τ as input from IFTOF experiments, we can readily estimate the capture coefficient of holes in *a*-Se. From Eq. (17), $C_t = e\mu_0 c / \epsilon$ so that with⁵⁰ $\mu_0 = 0.44 \text{ cm}^2 \text{ V}^{-1} \text{ s}^{-1}$ and $\epsilon_r = 6.5$, $C_t = 1.22 \times 10^{-7} \text{ cm}^3 \text{ s}^{-1}$. This value of C_t implies that the concentration of deep traps in *a*-Se must be $N_t = \mu_0 / \mu \tau' C_t \approx 5 \times 10^{11} \text{ cm}^{-3}$ which is a factor of ~ 20 less than typical integrated trap concentrations in *a*-Se determined by the cycled-up xerographic measurements both in this and previous works.³¹ It is therefore apparent that although the residual-potential model developed in this work can theoretically account for the low residual potential measured with respect to the KB universal curve, it requires the integrated concentration of deep-hole traps to be $5 \times 10^{11} \text{ cm}^{-3}$. Either the model is inadequate and needs further improvement (for example, the inclusion of release into the theory), or the integrated density of *a*-Se as determined from cycled-up experiments does not reflect the true trap concentration. The latter can arise, if during the xerographic cycling, more deep traps are created. In fact, this conjecture would totally account for the first-cycle xerographic and IFTOF experiments and also provide capture radii which are more in line with trapping into charged centers. The relationship between C_t and the capture radius for ballistic capture is⁴⁸

$$\pi r_b^2 = C_t e a / 6 \mu_0 k T = e^2 a c / \epsilon 6 k T, \quad (36)$$

which with $c \approx 1$ determined as above leads to 17 \AA . Clearly, such a capture radius is approximately what is expected if trapping occurs into an oppositely charged center, for example into a Se_1^- type of valence-alternation-pair (VAP) defect. For the diffusional case, C_t and the capture radius are related by⁴⁸

$$r_d = e C_t / 4 \pi \mu_0 k T = e^2 c / 4 \pi \epsilon k T, \quad (37)$$

which leads to a capture radius of 85 \AA . These capture radii are included in Table I as they are a direct result of the application of the model developed herein to the first residual and IFTOF measurements without invoking the cycled-up residual-potential result. The mechanisms that may cause deep-trap generation during the xerographic cycling need a detailed consideration of the physics of the xerographic cycle and are not addressed in this paper. It should be mentioned, however, that experiments have been recently reported where xerographic experiments with positive charging, immediately after negative charging, has resulted in much higher saturated residual potentials, indicating that during the negative xerographic cycling deep-hole traps were generated.⁵⁶ No accepted explanation currently exists for the observed phenomenon.

Another possibility for the major discrepancy may be that the lifetime value from the IFTOF measurement is much shorter than that relevant for xerographic measurements simply because the two experiments access different time scales. IFTOF experiments are usually carried out over a time scale on the order of $0.1\text{--}1 \text{ ms}$

whereas the xerographic measurement time scale is about $1\text{--}5 \text{ s}$. In an IFTOF study, traps with release times more than $\sim 1 \text{ ms}$ but less than 1 s will also contribute to τ whereas they will be invisible in xerographic experiments. The fact that V_R evinced no apparent dependence on the exposure times from 1 to 5 s (Fig. 9) indicates, however, that this is unlikely to be the reason for the discrepancy.

At present there is therefore no physically satisfactory theory to relate $\mu \tau'$ to the residual potential even though the latter is a reproducibly measured quantity reflecting the result of deep trapping during photodischarge. It is interesting to note that the Warter equation fortuitously corresponds to the $c = 1$ case of the rigorous theory and that it can predict the residual potential to within a factor of 2 given the $\mu \tau'$ product or vice versa. It therefore remains, at least empirically, to be a useful expression for estimating $\mu \tau'$ from a very simple xerographic measurement.

These are two mutually exclusive conclusions from the work. If the more rigorous deep-trapping kinematics model developed in this work is valid, then the combined study based on the first residual and IFTOF measurements lead to a deep-trap ballistic capture radius of $\sim 20 \text{ \AA}$, which is indicative of trapping into an oppositely charged center. Such charged centers occur naturally in chalcogenides amorphous semiconductors as a thermodynamic necessity of a negative Hubbard energy in these glasses.⁵⁷ As a corollary to this conclusion, one has to accept that cycled-up xerographic measurements do not reflect the true concentration of deep traps in the material, perhaps, due to trap generation during xerographic cycling.

If a combined study is made of IFTOF hole lifetime and cycled-up residual potential measurements, taking the latter as indicating the density of deep traps, then both the original KB theory and more rigorous KB theory developed herein must be considered as inadequate. The Warter expression then stands as a remarkably simple equation for determining the $\mu \tau'$ product from the first residual. The combined studies of IFTOF and cycled-up residual potential then lead to a ballistic capture radius of $\sim 3 \text{ \AA}$ which is indicative of neutral centers. The latter do not necessarily have to be paramagnetic neutral centers since an intimate valence-alternation pair (IVAP) would effectively look neutral to a drifting hole. The question that remains then is the following: "Could the capture radius of an IVAP be as small as 3 \AA ?" A related question arises from the application of the crystalline case equation to the calculation of the capture radius, i.e., r_c in Eq. (34). The capture radius in this case turns out to be $\sim 1 \text{ \AA}$ assuming a microscopic mobility of $0.44 \text{ cm}^2 \text{ V}^{-1} \text{ s}^{-1}$. If the microscopic transport process is in extended states below ξ_v , then the estimate for the mean carrier velocity is not drastically different from the thermal velocity so that r_c is unreasonably small simply because the value of μ_0 assumed in Eq. (34) may be not accurate. The estimate for μ_0 in *a*-Se supposes that the hole conduction mechanism in *a*-Se is shallow-trap-limited extended-state transport.⁵⁰ It is apparent from the present discussion that the calculation of the capture radius is strongly model dependent with

values in the range 2–20 Å as indicated in Table I. The values for the capture radii determined in this work encompasses trapping into neutral as well as charged centers.

The energy distribution of the deep traps shown in Fig. 18 indicates that the energy location of the peak is at 0.87 eV for *a*-Se and 0.9 eV for chlorinated *a*-Se:0.3 at. % As and does not depend on the preparation conditions. The position of the peak at 0.87 eV for *a*-Se is in agreement with the previously reported value.⁵¹ It can be seen that the changes from sample to sample are essentially in the peak value of the density of states. The half-energy widths $\Delta\xi$ of the density of states are approximately 0.06–0.07 eV, viz., $\sim 3kT$. This, in turn, means that the algorithm in Eq. (35) for evaluating $N(\xi)$ is at its useful limit since it applies to trap distributions which are wider than $3kT$. It should be remarked that the application of Eq. (35) to emission from a discrete set of traps at an energy ξ_0 results in a broad peak located at ξ_0 with an energy width $\sim 3kT$ so that when $N(\xi)$ versus ξ peaks from the xerographic data have such widths, the experiments cannot exclude trap emptying from a relatively discrete energy level.^{53,54} In the present case, the lack of a simple exponential decay for dV/dt versus t , as evidenced in Fig. 17, means that it is unlikely that hole emission is from a well-defined discrete level, leading, therefore, to the inference that the energy width of $N(\xi)$ versus ξ must be finite and less than $3kT$. Note that possible retrapping of emitted holes which occur at low voltages has been assumed negligible. The latter phenomenon would reduce the rate of emission and would therefore give the appearance of a broader distribution. Thus, the rate of decay of residual potential with time, when interpreted in terms of Simmon's formulation of emission kinetics, points to trap emptying from a very narrow-energy distribution of deep traps with a width less than $\sim 3kT$. It should be mentioned that Kubilius *et al.*⁵⁸ have also examined the rate of decay of the residual potential and have fitted to their results trap emptying from an exponentially decaying energy distribution of traps with a characteristic width parameter 0.05 eV. Although the results presented herein do not strictly support emission from an exponential density of states (see Fig. 17), which would result in a $dV/dt \sim t^{-n}$ type of decay, the total width of the distribution obtained by Kubilius *et al.*, $2W \sim 0.1$ eV, is comparable to that in Fig. 18.

VI. CONCLUSIONS

The Kanazawa and Batra model of deep-trapping kinetics in high-resistivity solids has been reformulated taking into account that the rate of trapping is proportional to the instantaneous concentration of empty traps. A new partial differential equation is derived that describes the space and time dependence of the electric field within the sample. With the appropriate boundary conditions, this partial differential equation is numerically solved and the final electric field in the specimen is obtained. It is found that the electric-field profile in the sample depends strongly on the capture radius-to-microscopic mobility ratio, $\epsilon C_i/e\mu_0$. The magnitude of

the field decreases and its spatial dependence becomes more linear as this ratio increases. By integrating the electric field, it is shown that the normalized residual potential (v_R) versus normalized trapping time (τ) behavior, i.e., the "universal curve," depends also on the $\epsilon C_i/e\mu_0$ ratio. Universal v_R versus τ curves parametric in the ratio $\epsilon C_i/e\mu_0$ have been derived which clearly show that first-cycle residual xerographic potential measurements cannot, in general, be used to determine the mobility-lifetime product of the charge carriers unless $\epsilon C_i/e\mu_0 \ll 1$.

Interrupted-field time-of-flight (IFTOF), first-cycle xerographic residual-potential (V_R), and cycled-up saturated xerographic residual-potential measurements ($V_{R\infty}$) were carried out on identical *a*-Se and Cl-doped *a*-Se:0.3 at. % As films. It was shown that the original Kanazawa-Batra universal curve is completely inadequate in describing the present experimental V_R versus $\mu\tau$ data, by as much as a factor of 5, whereas the theory developed herein can account for the experiments provided that the capture coefficient C_i is 1.22×10^{-7} cm³ s⁻¹ and that the deep-trap radius is ~ 17 Å for ballistic capture and 85 Å for diffusional capture. Although these radii are in line with the existence of charged trapping centers in chalcogenide glasses, the model requires an integrated density of deep traps that is a factor of 20 less than that determined at the end of cycled-up residual-potential measurements. The simple range-limited concepts of Warter leading to the expression $V_R = L^2/2\mu\tau'$ for the residual potential under weak-trapping conditions was found to predict the residual potential surprisingly well and to within a factor of 2.

By carrying out cycled-up xerographic residual-potential experiments on the same films for which the deep-trapping times have been determined from the IFTOF technique, the capture radius of deep-hole traps in *a*-Se and chlorinated *a*-Se:0.3 at. % As films were evaluated. Application of ballistic and diffusional trapping models to the IFTOF lifetime and cycled-up residual-potential data imply capture radii of 2–3 Å for both pure *a*-Se and Cl-doped 0.3 at. % As alloys. Furthermore, lifetime variations from sample to sample have been attributed to variations in the integrated trap concentration and not a change in the capture process.

The energy spectrum of the density of localized midgap states for both *a*-Se and Cl-doped *a*-Se:0.3 at. % As films were obtained via the xerographic-spectroscopy technique. The energy location of the peak of the localized density of states was at 0.87 eV for *a*-Se and 0.90 eV for Cl-doped *a*-Se:0.3 at. % As films, and insensitive to sample-to-sample variations. The density of states at the peak, however, was found to decrease with the hole lifetime. The energy width of the deep localized states was narrow and less than $\sim 3kT$ but not a single discrete level.

ACKNOWLEDGMENTS

We gratefully acknowledge many helpful and exciting discussions with Dr. M. Abkowitz (Xerox Corporation,

Webster, NY), who also suggested the initial study. The authors thank Michael Benson and John Davis at the Noranda Technology Centre (Pointe Claire, Quebec), for providing the selenium alloy source materials as well as supporting the project. One of the authors (B.P.) would like to express his gratitude to the CCR Division of

Noranda Minerals (East Montreal, Quebec) and the Noranda Technology Centre for financial support. This project was made possibly by research grants from the Natural Sciences and Engineering Research Council, Canada, and the Selenium-Tellurium Development Association Inc., Darien, CT.

- ¹M. D. Tabak, S. W. Ing, and M. E. Scharge, *IEEE Trans. Elec. Dev.* **ED-20**, 132 (1973).
- ²A. Madan and M. P. Shaw, *The Physics and Applications of Amorphous Semiconductors* (Academic, New York, 1988), Chap. 3 and references therein.
- ³I. P. Batra, K. Kanazawa, and H. Seki, *J. Appl. Phys.* **41**, 3416 (1970).
- ⁴I. Chen and J. Mort, *J. Appl. Phys.* **43**, 1164 (1972).
- ⁵C. C. Kao and I. Chen, *J. Appl. Phys.* **44**, 2708; **44**, 2718 (1973).
- ⁶J. Mort and I. Chen, *Applied Solid State Science* (Academic, New York, 1975, Vol. 5, p. 69, and references therein).
- ⁷P. J. Warter, *Appl. Opt. Suppl.* **3**, 65 (1969).
- ⁸K. K. Kanazawa and I. P. Batra, *J. Appl. Phys.* **43**, 1845 (1972).
- ⁹Fig. 1 of Ref. 8 is the Kanazawa-Batra universal curve.
- ¹⁰K. K. Kanazawa and I. P. Batra, *J. Non-Cryst. Solids*, **8-10**, 768 (1972).
- ¹¹W. E. Spear, *J. Non-Cryst. Solids* **1**, 197 (1969).
- ¹²F. K. Dolezalek, in *Photoconductivity and Related Phenomena*, edited by J. Mort and D. Pai (Elsevier, New York, 1976), Chap. 2.
- ¹³R. C. Enck and G. Pfister, in *Photoconductivity and Related Phenomena*, edited by J. Mort and D. Pai (Elsevier, New York, 1976), Chap. 7.
- ¹⁴J. M. Marshall, *Rep. Prog. Phys.* **46**, 1235 (1983).
- ¹⁵W. Ehrenberg and D. J. Gibbons, *Electron Bombardment Induced Conductivity and Its Applications* (Academic, New York, 1981).
- ¹⁶Reference 2, Chap. 2.
- ¹⁷K. C. Kao and W. Hwang, *Electrical Transport in Solids in Particular Reference to Organic Semiconductors* (Pergamon, New York, 1981).
- ¹⁸Z. Hecht, *Z. Phys.* **77**, 235 (1932).
- ¹⁹See, for example, W. E. Spear and J. Mort, *Proc. Soc.* **81**, 130 (1963).
- ²⁰R. A. Street, *Appl. Phys. Lett.* **41**, 1060 (1982).
- ²¹R. A. Street, J. Zesch, and M. J. Thomson, *Appl. Phys. Lett.* **43**, 1425 (1983).
- ²²R. A. Street, J. Zesch, and M. J. Thomson, *Appl. Phys. Lett.* **43**, 672 (1983).
- ²³R. A. Street, C. C. Tasi, M. Stutzman, and J. Kakalios, *Philos. Mag.* **56**, 289 (1987).
- ²⁴D. J. Gibbons and W. E. Spear, *J. Phys. Chem. Solids* **27**, 1917 (1966).
- ²⁵W. E. Spear, W. E. Steemers, and H. Mannsperger, *Philos. Mag. B* **48**, L49 (1983).
- ²⁶See also H. Ehrenberg, and D. J. Gibbons, Ref. 15, Chap. 5.
- ²⁷S. L. Kasap, R.P.S. Thakur, and D. Dodds, *J. Phys. E* **21**, 1195 (1988).
- ²⁸S. O. Kasap, B. Polischuk, and D. Dodds, *Rev. Sci. Instrum.* **61**, 2081 (1990).
- ²⁹S. O. Kasap, V. Aiyah, B. Polischuk, and M. Abkowitz, *Philos. Mag. Lett.* **62**, 377 (1990).
- ³⁰D. M. Pai, 4th International Conference on Non-Impact Technologies, SPSE, New Orleans, 1988 (SPSE, Springfield, VA, 1988), p. 20.
- ³¹M. Abkowitz and R. C. Enck, *Phys. Rev. B* **25**, 2567 (1982).
- ³²M. Okuda, K. Motomura, H. Naito, T. Matsushita, and T. Nakau, *Jpn. J. Appl. Phys.* **21**, 1127 (1982).
- ³³M. Abkowitz and R. C. Enck, *Phys. Rev. B* **27**, 7402 (1983).
- ³⁴F. Carasco, J. Mort, F. Jansen, and S. Grammatica, *J. Appl. Phys.* **57**, 5306 (1985).
- ³⁵J. Mort, S. Grammatica, J. C. Knights, and R. Lugan, *Solar Cells* **2**, 451 (1980).
- ³⁶M. E. Scharfe, *Electrophotography Principles and Optimization* (Wiley, New York, 1984), Chap. 4.
- ³⁷B. Polischuk and S. O. Kasap, *Measur. Sci. Technol.* (to be published).
- ³⁸S. O. Kasap, B. Polischuk, Viswanath, Aiyah, and S. Yannacopoulos, *J. Appl. Phys.* **67**, 1918 (1990).
- ³⁹J. S. Berkes, *Electrophotography: Second International Conference*, edited by D. R. White (SPSE, Springfield, VA, 1974), p. 137.
- ⁴⁰M. D. Tabak and W. J. Hillegas, *J. Vac. Sci. Technol.* **9**, 387 (1972).
- ⁴¹J. C. Schottmiller, *J. Vac. Sci. Technol.* **12**, 807 (1975).
- ⁴²R. B. Stephens, *J. Appl. Phys.* **49**, 5855 (1978).
- ⁴³M. Abkowitz, *Ann. N.Y. Acad. Sci.* **371** (1981).
- ⁴⁴M. Abkowitz, *J. Non-Cryst. Solids* **66**, 315 (1984).
- ⁴⁵M. Abkowitz, *Polymer Eng. Sci.* **24**, 1149 (1984).
- ⁴⁶M. Abkowitz, *J. Non-Cryst. Solids* **77&78**, 1191 (1985).
- ⁴⁷S. O. Kasap, B. Polischuk, D. Dodds, and S. Yannacopoulos, *J. Non-Cryst. Solids* **114**, 106 (1989).
- ⁴⁸R. A. Street, *Philos. Mag. B* **49**, L15 (1984).
- ⁴⁹T. R. Waite, *Phys. Rev.* **107**, 463 (1957).
- ⁵⁰M. Abkowitz and D. Pai, *Phys. Rev. B* **18**, 1741 (1978).
- ⁵¹M. Abkowitz and J. M. Markovics, *Philos. Mag. B* **49**, L31 (1984).
- ⁵²J. G. Simmons and L. S. Wei, *Solid State Electron.* **17**, 117 (1974).
- ⁵³J. G. Simmons and G. W. Taylor, *Solid State Electron.* **17**, 1125 (1974).
- ⁵⁴J. G. Simmons and M. C. Tam, *Phys. Rev. B* **7**, 3706 (1973).
- ⁵⁵H. Naito, K. Motomura, M. Okuda, T. Nakau, and T. Matsushita, *Jpn. J. Appl. Phys.* **22**, L531 (1983).
- ⁵⁶B. E. Springett, in the *Proceedings of the 4th International Symposium on Uses of Selenium and Tellurium, Banff, 1989* (Selenium-Tellurium Development Association, Inc., Darien, CT, 1989), p. 126.
- ⁵⁷S. R. Elliot, *Physics of Amorphous Materials* (Longman, London, 1983), Chap. 6 and references therein.
- ⁵⁸A. Kubilius, Br. Petretis, V. I. Arkhipov, and I. A. Rudenko, *J. Non-Cryst. Solids* **87**, 290 (1986).